ACS APPLIED MATERIALS & INTERFACES

Research Article

www.acsami.org

Plasmonic AuNP/g-C_3N_4 Nanohybrid-based Photoelectrochemical Sensing Platform for Ultrasensitive Monitoring of Polynucleotide Kinase Activity Accompanying DNAzyme-Catalyzed Precipitation Amplification

Junyang Zhuang, Wenqiang Lai, Mingdi Xu, Qian Zhou, and Dianping Tang*

Key Laboratory of Analysis and Detection for Food Safety (MOE & Fujian Province), Institute of Nanomedicine and Nanobiosensing, Department of Chemistry, Fuzhou University, Fuzhou 350108, People's Republic of China

Supporting Information

ABSTRACT: A convenient and feasible photoelectrochemical (PEC) sensing platform based on gold nanoparticles-decorated g-C_3N_4 nanosheets (AuNP/g-C_3N_4) was designed for highly sensitive monitoring of T4 polynucleotide kinase (PNK) activity, using DNAzyme-mediated catalytic precipitation amplification. To realize our design, the AuNP/g-C_3N_4 nanohybrid was initially synthesized through in situ reduction of Au(III) on the g-C_3N_4 nanosheets, which was utilized for the immobilization of hairpin DNA_1 (HP_1) on the sensing interface. Thereafter, a target-induced isothermal amplification was automatically carried out on hairpin DNA_2 (HP_2) in the solution phase through PNK-catalyzed 5′-phosphorylation accompanying formation of numerous trigger DNA fragments, which could induce generation of hemin/G-quadruplex-based DNAzyme on hairpin DNA_1. Subsequently, the DNAzyme could catalyze the 4-chloro-1-naphthol (4-CN) oxidation to produce an insoluble precipitation on the AuNP/g-C_3N_4 surface, thereby resulting in the local alternation of the photocurrent. Experimental results revealed that introduction of AuNP on the g-C_3N_4 could cause a ~100% increase in the photocurrent because of surface plasmon resonance-enhanced light harvesting and separation of photogenerated e^-/h^+ pairs. Under the optimal conditions, the percentage of photocurrent decrement ($\Delta I/I_0$, relative to background signal) increased with the increasing PNK activity in a dynamic working range from 2 to 100 mU mL^{-1} with a low detection limit (LOD) of 1.0 mU mL^{-1}. The inhibition effect of adenosine diphosphate also received a good performance in PNK inhibitor screening research, thereby providing a useful scheme for practical use in quantitative PNK activity assay for life science and biological research.

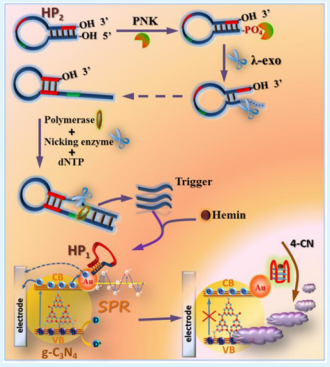

KEYWORDS: *photoelectrochemistry, gold-decorated g-C_3N_4 nanosheets, surface plasmon resonance, T4 polynucleotide kinase, isothermal amplification*

1. INTRODUCTION

The photoelectrochemical (PEC) sensing approach is a newly emerged yet dynamically developing technique for various biological assays including antigens or antibodies,[1−3] nucleic acids,[4,5] proteins[6] and cells.[7,8] Evolved from the traditional electrochemical detection method, the PEC-based sensing strategy can preserve the essential benefits of the former in sensitivity, robustness, broad applicability, and suitability to automation.[9,10] Nowadays, designs of PEC sensors mainly depend on the photoactive metallic semiconductors (e.g., TiO_2, CdS, WO_3 and ZnO) based on their high-efficiency photoelectric conversion elements and biocompatible immobilization matrices for biomolecules. Unfavorably, the potentially practical application of metallic semiconductors in the PEC sensors is still restricted, e.g., some semiconductors with the wide band gap (e.g., 3.2 eV for TiO_2) are of strong oxidizing properties and require for high-energy excitation light sources (e.g., UV light) or suffer from photocorrosion under illumination, thus easily resulting in fatal damage toward biomolecules or the instability of the sensors.[11−13] Despite some advances in this field, the quest for new PEC sensing platforms continues as both the clinical diagnostic and life science research communities constantly look from assay technologies that are sensitive, robust and easy to implement.

Graphitic-phase carbon nitride (g-C_3N_4), a metal-free photoactive semiconductor consisting of abundant and nontoxic elements, has attracted worldwide attention due to its superior photocatalytic activity[14] and potential applications in chemical and biosensing.[15−17] Moreover, g-C_3N_4 is also a green and stable nanostructure with medium oxidation capacity, visible-light response owning to its relatively narrow band gap (2.7 eV). Compared with bulk g-C_3N_4, graphene-analogue g-C_3N_4 nanosheets are of improved photocatalytic activity and photocurrent response based on the quantum confinement effect, higher electron−hole separation efficiency, larger surface area and better electronic conductivity.[18,19] Unfortunately, the

Received: March 3, 2015
Accepted: April 2, 2015
Published: April 2, 2015

DOI: 10.1021/acsami.5b01923
ACS Appl. Mater. Interfaces 2015, 7, 8330−8338

Scheme 1. (A) Mechanism of the Photocurrent Production on the AuNP/g-C_3N_4 Nanohybrid under Visible-Light Irradiation (CB, conduction band; VB, valence band). (B) Schematic Illustration of Double Hairpins-based Photoelectrochemical Detection Platform toward Monitoring the PNK Activity on AuNP/g-C_3N_4 Nanohybrid-Modified Electrode Coupling with an Isothermal Amplification Strategy and an Enzymatic Biocatalytic Precipitation Technique

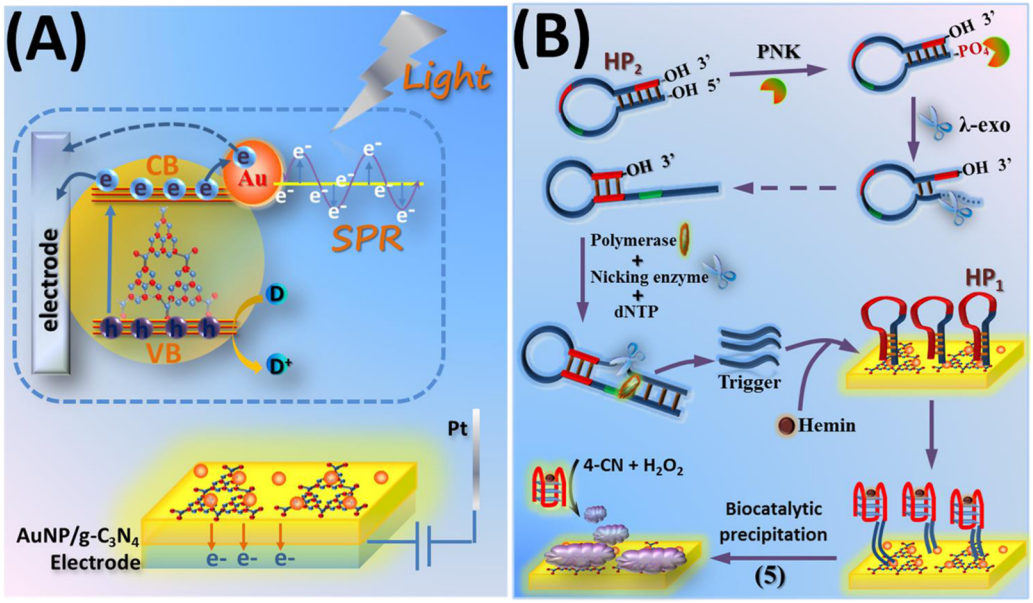

visible-light absorption, the separation of photogenerated electron–hole (e^-/h^+) pairs and the resulting photoelectrochemical response is relatively limited to some extent.

Surface plasmonic resonance (SPR) phenomenon in metallic nanostructures (e.g., nanogold and nanosilver) is of interest for a variety of applications owing to the large electromagnetic field enhancement that occurs in the vicinity of the metal surface, and the dependence of resonance wavelength on the nanoparticle's size, shape and local dielectric environment. Actually, this well-established optical phenomenon of metallic nanostructure has facilitated the development of various optical sensing methods, namely, surface plasmonic resonance sensors.[20] Besides, the combination of plasmonic metal with semiconductor has become a flexible routine for enhancing the photocatalytic activity and photocurrent response of semiconductor nanostructures. This phenomenon is also known as SPR enhanced photocatalysis based on the electrical field amplification effect, enhanced light absorbance and interfacial charge transfer in semiconductor/metal interface.[21−23] In this regards, our motivation is exploring a highly efficient photoelectrochemical sensing platform by using nanogold-decorated g-C_3N_4 nanosheets as the signal-transduction tags because plasmonic metal–semiconductor systems with a SPR-enhanced effect can effectively generate the photocurrent as a detection signal.

The T4 polynucleotide kinase (PNK) that catalyzes the phosphorylation of nucleic acids at the 5′-hydroxyl termini plays a crucial role in regulation of many important cellular events, particularly in the cellular responses to nucleic acid strand damage and interruption.[24,25] As a proof-of-concept, herein we present a novel and highly sensitive PEC assay method for quantitative monitoring of T4 PNK activity based on the gold nanoparticles-decorated g-C_3N_4 nanosheets (AuNP/g-C_3N_4) coupling with a double-hairpin-based isothermal amplification strategy and DNAzyme-assisted biocatalytic precipitation (Scheme 1). Initially, the added PNK catalyzes the phosphorylation reaction at the 5′-termini of hairpin DNA_2 in the solution phase to induce the progression of isothermal amplification accompanying the formation of the trigger DNA fragment. And then, the generated trigger DNA fragment can activate the hemin/G-quadruplex-based DNAzyme sequence at the immobilized hairpin DNA_1 on the AuNP/g-C_3N_4 PEC electrode by opening the hairpin structure. Finally, the activated DNAzyme catalyzes the oxidization of 4-chloro-1-naphthol (4-CN) to generate an insoluble/insulating precipitate on the AuNP/g-C_3N_4, thereby directly blocking the light harvesting and destroying the plasmonic structure of AuNP/g-C_3N_4. Consequently, the photocurrent of AuNP/g-C_3N_4-based sensing platform is gradually inhibited with the increasing PNK activity. By monitoring the change in photocurrent, we can quantitatively determine the PNK activity in the sample. The aim of this work is to successfully transform the AuNP/g-C_3N_4 nanohybrid into a versatile photoelectrochemical detection platform for highly sensitive monitoring of PNK activity.

2. EXPERIMENTAL SECTION

Materials and Chemicals. T4 polynucleotide kinase (PNK), N.BbvC IA endonuclease, λ exonuclease (λ-exo) and CutSmart buffer were purchased from New England Biolabs (NEB, UK). Adenosine triphosphate (ATP), dNTP, dicyanamide and $HAuCl_4{\cdot}3H_2O$ were acquired from Sigma-Aldrich (Shanghai, China). Klenow fragment exo^- (KF exo^-) and hemin were achieved from Thermo Fisher Sci. Inc. (Waltham, MA). All other chemicals used in this work were of analytical grade. Ultrapure water used was from a Mill-Q water purification system (18.2 MΩ cm^{-1}, Millipore). All the oligonucleotides were custom-synthesized by Sangon Inc. (Shanghai, China), and purified by high-performance liquid chromatography and confirmed by mass spectrometry. The sequences of the oligonucleotides were listed as follows

Hairpin DNA_1 (HP_1): 5′-**GGGTAGGGCGGGTTGGGATG**AG-AAAGGGCTGCCA*CATCCCAACCCATA*-SH-3′.

DOI: 10.1021/acsami.5b01923
ACS Appl. Mater. Interfaces 2015, 7, 8330−8338

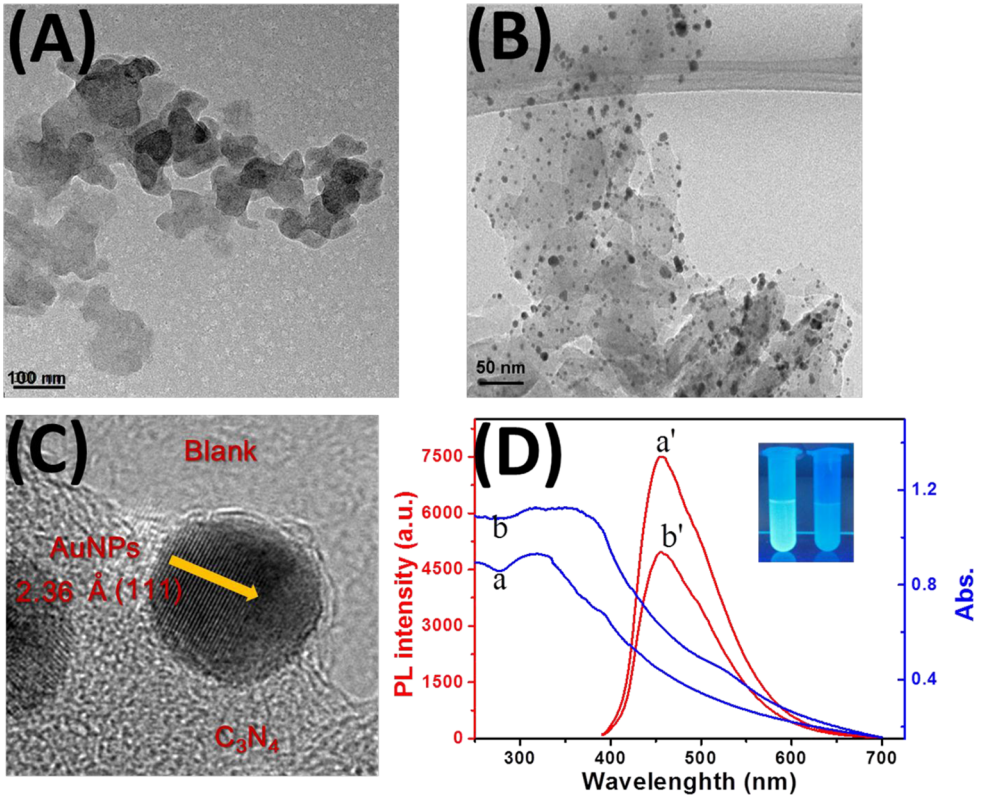

Figure 1. TEM images of (A) g-C_3N_4 nanosheets and (B) AuNP/g-C_3N_4 nanohybrids [Note: (C) HRTEM image of AuNP/g-C_3N_4 nanohybrids]. (D) UV−vis absorption spectra (blue line) and photoluminescence (PL) spectra (red line) of (a) g-C_3N_4 nanosheets and (b) AuNP/g-C_3N_4 nanohybrids [Insets: photographs of (a) g-C_3N_4 nanosheets and (b) AuNP/g-C_3N_4 nanohybrids obtained under excitation at 365 nm].

Hairpin DNA_2 (HP_2): 5′-HO-CTAACTCGCACTACTA-*CGGTTTGGCTGCCACATCCCAACCCA TACCTCAGCTC* TAACTCGCAGGCTAGTAGTGCGAGTTAG-OH-3′.

In the HP_1, the underlined letters were the stem of hairpin probe and the italic letters were the recognition region for the trigger DNA fragment while the bold letters were the sequence of hemin/G-quadruplex-based DNAzyme. In the HP_2, the underlined letters were the stem of hairpin probe and the complementary sequences of the bold italic letters were the recognition-site for N.BbvC IA endonuclease whereas the italic letters were the template sequence for polymerization reaction.

Synthesis of g-C_3N_4 and AuNP/g-C_3N_4. Prior to synthesis, the bulk g-C_3N_4 was prepared by heating dicyanamide at 600 °C for 2 h in static air with a ramp of ∼3 °C min^{-1}. Following that, the resulting yellow agglomerates were cooled down at ∼1 °C min^{-1}, and milled into powder by a mortar. Afterward, the g-C_3N_4 nanosheets were obtained by liquid exfoliation of the bulk g-C_3N_4 powder in water. Briefly, 600 mg of bulk g-C_3N_4 powder was dispersed into 100 mL of distilled water and sonicated for 10 h. The residual unexfoliated bulk g-C_3N_4 was removed by centrifugation at 4500*g*. Subsequently, the supernatant was further centrifuged at 8000*g*, and the obtained precipitation was dried at 45 °C in a vacuum oven. The molecular structure of the as-prepared g-C_3N_4 nanosheets were characterized using Fourier-transform infrared spectroscopy (FT-IR) (Figure S1 in the Supporting Information).

Next, the as-synthesized g-C_3N_4 was utilized for the preparation of AuNP/g-C_3N_4 according to the previous report with a slight modification.[26] Initially, 20 μL of 10 mM $HAuCl_4$ aqueous solution was added to 5 mL of g-C_3N_4 suspension (∼2.0 mg mL^{-1}) and stirred for 2 h in the dark. And then, 30 μL of 0.01 M freshly prepared $NaBH_4$ was added dropwise to the suspension for the reduction of Au(III). The resulted suspension was continuously stirred until the gas evolution of $NaBH_4$ ceased. Following that, the suspension was centrifuged at 6000*g* in order to remove the unreacted/unbound species including single gold nanoparticle. Finally, the obtained AuNP/g-C_3N_4 was washed with distilled water, and redispersed into 5 mL of distilled water for further use.

Fabrication of AuNP/g-C_3N_4-based PNK Sensing Platform. Initially, a glassy carbon electrode (GCE, 2 mm in diameter) was polished with 0.3 and 0.05 μm alumina slurry in turn, followed by successive sonication in water and ethanol and then dried under nitrogen. Following that, 4 μL of the above-prepared AuNP/g-C_3N_4 suspension was dropped onto the cleaned GCE and dried at room temperature. After washing with distilled water, the AuNP/g-C_3N_4-modifed GCE was used for the conjugation of HP_1 through the interaction of its 3′-terminal thiol group with the decorated gold nanoparticles on the g-C_3N_4 nanosheets (Note: before the assembly, probe HP_1 was dispersed into 10 mM tris(2-carboxyethyl)phosphine for 60 min to reduce any disulfides between DNA molecules). Briefly, the AuNP/g-C_3N_4-modifed GCE was immersed into 10 mM Tris−HCl buffer (pH 7.4) containing 1.0 μM treated HP_1, and incubated for 4 h at room temperature. Subsequently, the resulting electrode was reincubated with 6-mercapto-1-hexanol (1.0 mM) for 60 min under the same conditions to passivate the remaining gold surface and block possible active sites. The remaining area and active site on the uncovered g-C_3N_4 were also blocked by 1% BSA. Finally, the HP_1/AuNP/g-C_3N_4/GCE was immersed into 10 mM Tris−HCl buffer (pH 7.4) containing 0.5 M NaCl and 20 mM $MgCl_2$ at 4 °C for further use.

Monitoring of PNK Activity. Scheme 1 gives the monitoring mechanism of PNK activity and photoelectrochemical measurement procedure on the AuNP/g-C_3N_4-modified electrode by coupling with DNAzyme-catalyzed precipitation reaction. Photocurrent measurement was carried out on a homemade detection equipment with a 500 W Xe lamp and a 400 nm cutoff filter (as the light source to provide the visible irradiation) at a constant potential of 0.2 V in 0.1 M Na_2SO_4 solution containing 0.1 M Na_2S and 0.05 M Na_2SO_3. All electrochemical measurements including impedimetric spectroscope (EIS) were performed on an AutoLab electrochemical workstation (μAUTIII.FRA2.v, Eco Chemie, The Netherlands) with a conventional three-electrode system including an AuNP/g-C_3N_4-modified

DOI: 10.1021/acsami.5b01923
ACS Appl. Mater. Interfaces 2015, 7, 8330−8338

working electrode, a Pt-wire counter electrode and an Ag/AgCl reference electrode. The assay mainly consisted of the following steps: (i) The PNK sample with certain concentration was initially incubated with 10 μL of Tris−HCl buffer (10 mM, pH 8.0) containing 25-nM HP_2, 1.0 mM ATP, 14 units λ-exo, 10 mM $MgCl_2$ and 5.0 mM dithiothreitol for 35 min at 37 °C, and the reaction was then terminated through heating the mixture to 90 °C followed by cooling to room temperature (Note: during this process, the added PNK catalyzed the phosphorylation at the 5′-termini hydroxy group of HP_2, followed by selective hydrolysis at its stem region by λ-exo to form a new hairpin probe); (ii) 4 μL of CutSmart buffer (including 0.6 mM dNTP, 1.0 U Klenow fragment exo^- and 1.8 U N.BbvC IA endonuclease) and 6 μL distilled water were added to the mixture, and the mixture was incubated for 70 min at 37 °C, followed by cooling to 4 °C (Note: during this process, a large number of trigger DNA fragments were formed by enzyme-assisted isothermal reaction); (iii) 4.0 μL of the above-reacted product and 2 μM hemin were dropped on the HP_1/AuNP/g-C_3N_4/GCE in sequence, and incubated for 30 min at 37 °C (Note: during this process, peroxidase-mimicking DNAzyme was formed); (iv) the resulting electrode was dipped into 0.1 M PBS (pH 7.4) containing 1.0 mM 4-CN and 0.15 mM H_2O_2 to induce DNAzyme-based biocatalytic precipitation reaction. Finally, the resulting electrode was introduced to photocurrent measurement referring to above-mentioned assay system.

3. RESULTS AND DISCUSSION

Characterization of AuNP/g-C_3N_4 Nanohybrid. In this work, the photocurrent mainly derives from the immobilized AuNP/g-C_3N_4 on the sensing interface. One important precondition for the development of PEC sensor is to successfully synthesize the high-efficient AuNP/g-C_3N_4 with enhanced photocurrent generation. Initially, we used transmission electron microscopy (TEM) to investigate the morphology and surface structure of the as-synthesized g-C_3N_4 before and after modification with nanogold particles. Figure 1A displays the typical TEM image of g-C_3N_4, and the morphology of the synthesized g-C_3N_4 was planar sheet-like with an average size of 100−150 nm, indicating that the nanosheets were successfully formed. It is well-known that the layer structures were derived from the graphitic planes with a conjugated aromatic system of tristriazine units.[27] Significantly, we also observed that many nanoparticles were uniformly covered on the surface/edges of g-C_3N_4 nanosheets after in situ reduction of Au(III) by the added $NaBH_4$ (Figure 1B). However, a puzzling question arises, as the fact whether the nanoparticles originated from zero Au^0. To verify this concern, we used high-resolution TEM (HRTEM) to study the nanohybrids. As indicated from Figure 1C, the nanoparticles displayed the lattice fringes with an interplane distance of 2.36 Å corresponding to the (111) lattice space of metallic gold, suggesting that the formed nanoparticles were single gold crystals.[28] More importantly, a distinguishable interface was observed to formed between g-C_3N_4 and AuNP. Such an interface formed between plasmonic metal nanoparticles and semiconductor was known to be highly beneficial for the electron transfer within the composite structure and the separation of photoinduced e^-/h^+ pairs.

To realize our design on the subsequent application of AuNP/g-C_3N_4 in the PEC sensor, we compared the optical properties of g-C_3N_4 with AuNP/g-C_3N_4 by using UV−vis absorption spectroscopy and photoluminescence spectroscopy, respectively (Figure 1D). Compared with g-C_3N_4 alone (curve a), an obscure absorption peak at ∼520 nm for the characteristic peak of colloidal gold SPR band could be appeared for the AuNP/g-C_3N_4 (curve b). The light absorption of AuNP/g-C_3N_4 in UV region also increased distinctly, which might be attributed to the inherent light absorption of nanogold in the UV region.[29] Hence, it could be determined that introduction of AuNP with g-C_3N_4 exhibited an enhanced light harvesting, which could play a positive role in enhancing the photocurrent response (curve b vs curve a). Because the photoluminescence of semiconductors was generated during the recombination process of e^-/h^+ pair and there was a positive correlation between the photoluminescence intensity and recombination rate (Note: high photoluminescence intensity indicated a high recombination rate and a weak photocurrent response), the photoluminescence spectra could be employed to investigate the recombination rate of the photogenerated e^-/h^+ pairs. Further, both g-C_3N_4 (curve a) and AuNP/g-C_3N_4 (curve b) displayed a luminescence peak at ∼455 nm, which was attributed to the band−band photoluminescence phenomenon with the energy of emission light approximately equal to the band gap energy of g-C_3N_4 (2.7 eV).[30] Notably, photoluminescence intensity of the latter was observed to be much lower, which indicated that the separation of photogenerated e^-/h^+ pairs in AuNP/g-C_3N_4 was more efficient, and the recombination of e^-/h^+ pairs was inhibited because the excited electron directly transported from the conduction band (CB) of g-C_3N_4 to AuNP through the interface between them.

As described above, the SPR-enhanced photoactive nanostructures with improved visible-light absorbance and e^-/h^+ pair separation efficiency could be successfully established by the combination of plasmonic AuNP with the g-C_3N_4. To further clarify the amplified efficiency of the as-synthesized AuNP/g-C_3N_4 toward generation of photocurrent, two nanostructures including g-C_3N_4 and AuNP/g-C_3N_4 (the same-amount g-C_3N_4 used in this case) were directly immobilized onto the cleaned GCE, respectively. As shown from Figure 2, the presence of AuNP on the g-C_3N_4 nanosheets

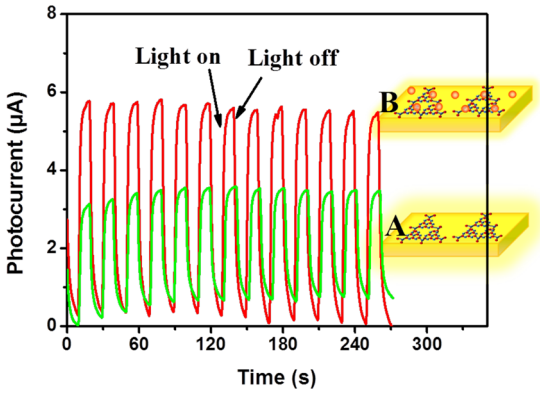

Figure 2. Photocurrent responses for (A) g-C_3N_4 nanosheets and (B) AuNP/g-C_3N_4 nanohybrids. All the electrodes were evaluated at a constant potential of 200 mV (vs Ag/AgCl) in 0.1 M Na_2SO_4 solution containing 0.1 M Na_2S and 0.05 M Na_2SO_3 under visible-light irradiation.

could cause a ∼100% increase in the photocurrent relative to g-C_3N_4-modified electrode alone. Scheme 1A represents the production mechanism of photocurrent in the AuNP/g-C_3N_4. The visible-light fallen on the surface of AuNP/g-C_3N_4 initially excites the generation of conduction band electrons (e^-) and valence band (VB) holes (h^+) in g-C_3N_4. Owning to the SPR-enhanced effect, the excited electrons rapidly transports from

DOI: 10.1021/acsami.5b01923
ACS Appl. Mater. Interfaces 2015, 7, 8330−8338

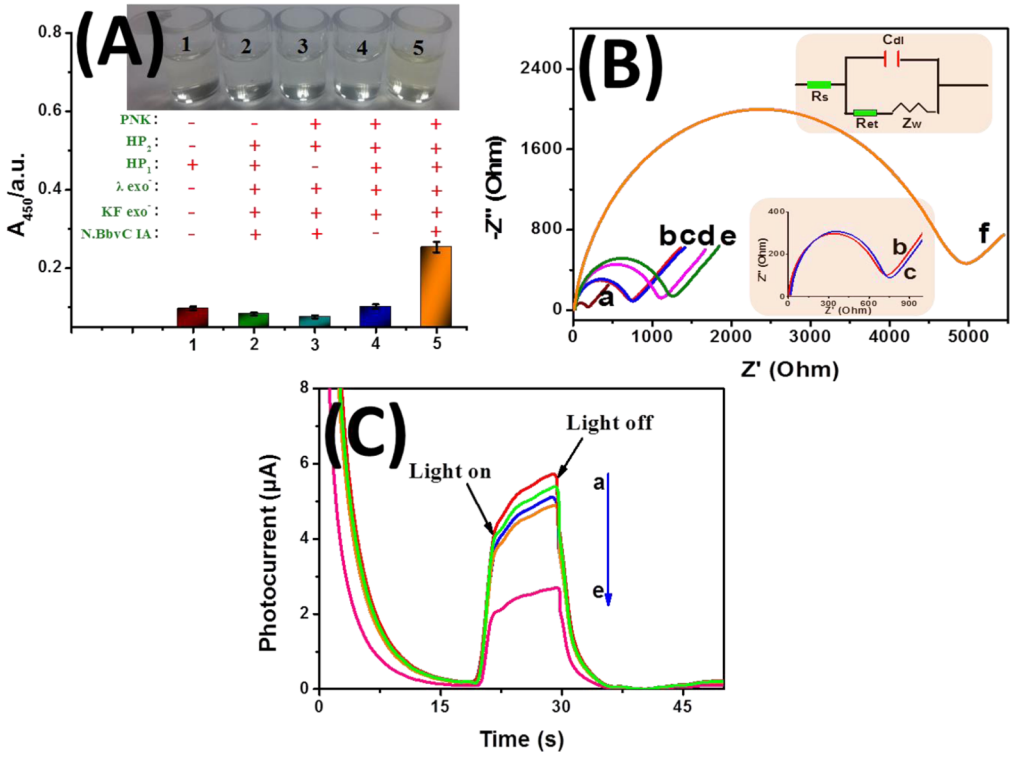

Figure 3. (A) UV−vis absorbance intensities of different components (+, with; −, without) relative to TMB-H_2O_2 system (Insets: photographs) (Note: hemin was used in this case). (B) EIS spectra of (a) AuNP/g-C_3N_4-modified electrode, (b) sensor a + HP_1, (c) sensor b + 4-CN + H_2O_2, (d) sensor b after reaction with the trigger DNA fragment, (e) sensor d + hemin, and (f) sensor e + 4-CN + H_2O_2 in 0.1 M KCl containing 5.0 mM $K_3Fe(CN)_6/K_4Fe(CN)_6$ (Insets: the corresponding equivalent circuit and the magnificent figures of curves b and c). (C) Photocurrent responses of (a) AuNP/g-C_3N_4-modified electrode, (b) sensor a + HP_1 + MCH/BSA, (c) sensor b after reaction with PNK-induced isothermal amplification, (d) sensor c + hemin and (e) sensor d + 4-CN + H_2O_2 (50 mU mL^{-1} used in this case).

the CB of g-C_3N_4 to AuNP through the interface built between g-C_3N_4 and AuNP, which in turn promoted the separation of e^-/h^+ pairs.[31] As a consequence, a large number of electrons accumulated in the CB of g-C_3N_4 and on the surface of AuNP. These electrons then rapidly transferred to electrode, causing a higher photocurrent.

Characteristics of AuNP/g-C_3N_4-based PNK Sensing Platform. To adequately highlight the advantages of the as-synthesized AuNP/g-C_3N_4 for development of photoelectrochemical sensors, the system was utilized for quantitative screening of PNK activity by coupling with two hairpin probes (HP_1 and HP_2) and enzymatic biocatalytic precipitation amplification (Scheme 1B). The thiolated HP_1 probe containing a sequence of hemin/G-quadruplex-based DNAzyme (Aim: for the formation of hemin/G-quadruplex-based peroxidase-mimicking DNAzyme) was immobilized onto the AuNP/g-C_3N_4-modified electrode through the Au−S bond (Note: the hemin/G-quadruplex DNAzyme sequence was partially caged in the stem region of HP_1 at this step, and could not fold into the catalytically active DNAzyme regardless of the presence of hemin or not). Upon formation of the trigger DNA fragment, the trigger sequence could open HP_1 probe, and release the caged DNAzyme sequence to construct the peroxidase-mimicking DNAzyme in the presence of hemin. In contrast with probe HP_1, the immobilization-free HP_2 (working in the solution reaction) could recognition the phosphorylation of target PNK and mediate the enzyme-assisted isotherm amplification reaction in the solution phase. Each HP_2 probe had a stem of 16 base pairs (bp) enclosing a 49-nucleotide (nt) loop with a blunt end. The initial 10 bases at the 3′ end of HP_2 (TGCGAGTTAG, denoted as unit I) could not only pair with the initial 10 bases (CTAACTCGCA) of its 5′ end, but also was the complementary sequences of 10 bases (CTAACTCG-CA, denoted as unit II) in the middle of loop region. Logically, a confused question was which one unit I should initially hybridize with. From a thermodynamic point of view, the hairpin probe with a 16-bp stem was more stable than that of 10 bp according to the Nucleic Acid Package calculation (see Figure S2 and a related description in the Supporting Information). In addition, the recognition sequence of N.BbvC IA endonuclease was close to unit II at the loop (CCTCAGCT, denoted as unit III), while the complementary sequence of the trigger DNA fragment located at its 5′ end (denoted as unit IV) (Note: the produced trigger DNA sequence could hybridize partially with the immobilized HP_1 on the AuNP/g-C_3N_4 to release the caged DNAzyme sequence).

Upon PNK introduction, the target analyte initially catalyzed the transfer of the γ-phosphate residue of ATP to 5′-hydroxyl termini of HP_2, resulting in the 5′-phosphorylated HP_2. With the help of λ-exo, the 5′ phosphorylated strand at the double-helical stem of HP_2 was digested selectively from the 5′-phosphate termini,[32] thus resulting in the dissociation of unit I from the double-stranded DNA. Alternatively, the released unit I could pair with unit II to form a new hairpin DNA with an extra overhang including units III and IV at the 5′ end, which was conducive for polymerase/nicking enzyme-assisted isotherm amplification reaction without the participation of exogenous primers because unit I with 3′-OH could act as an endogenous primer to initiate the KF exo^--based polymerization reaction by using the overhang region as template. With

DOI: 10.1021/acsami.5b01923
ACS Appl. Mater. Interfaces 2015, 7, 8330−8338

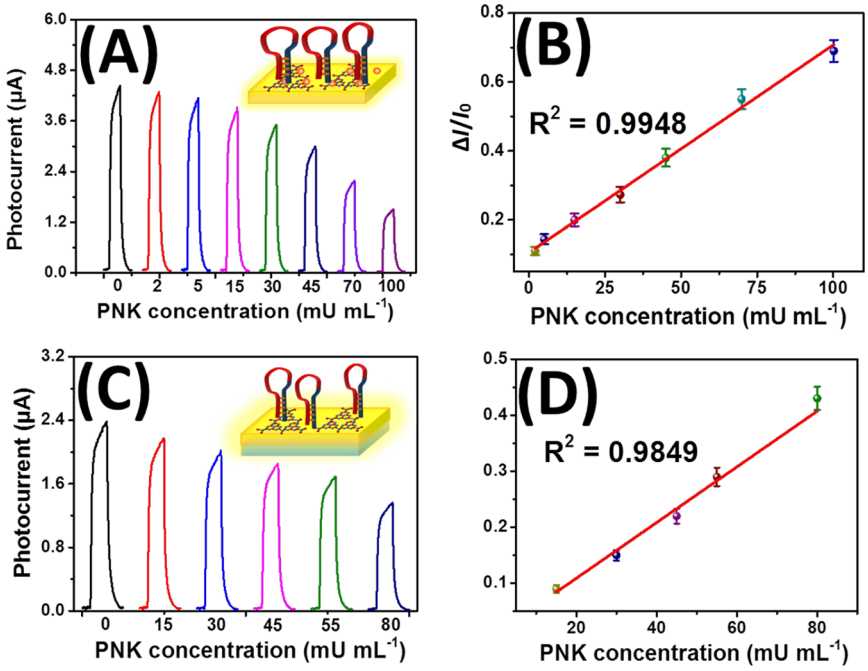

Figure 4. (A,C) Photocurrent responses and (B,D) the corresponding calibration curves of double hairpins-based detection platform toward different PNK Activities on (A,B) AuNP/g-C_3N_4-coated electrode and (C,D) g-C_3N_4-coated electrode [Note: $\Delta I = I_0 - I$, I_0 was the background photocurrent of HP_1-modified GCE, and I was the photocurrent of finishing all steps].

the assistance of N.BbvC IA endonuclease, numerous trigger DNA fragments were generated on the basis of the isothermal amplification reaction. The as-produced trigger DNA fragments could hybridize with the immobilized HP_1 on the electrode, thereby leading to the formation of numerous DNAzyme biomolecules based on the above-described procedure. The formed DNAzyme could catalyze 4-chloro-1-naphthol (4-CN) oxidization by H_2O_2 to yield an insoluble/insulating benzo-4-chlorohexadienone precipitate on the AuNP/g-C_3N_4 surface, thus inhibiting the production of the photocurrent. By monitoring the change in the photocurrent, we could indirectly determine the PNK activity in the sample with high sensitivity.

To realize our design, two key points to be investigated in the strategy were (i) whether target PNK could induce HP_2-based isothermal amplification reaction to activate the peroxidase-mimicking DNAzyme at the probe HP_1 and (ii) whether the as-produced DNAzyme could catalyze the 4-CN precipitation reaction to inhibit the photocurrent. To demonstrate the first issue, we used UV−vis absorption spectroscope to investigate the characteristics of different substrates after incubation with various components relative to 3,3′,5,5′-tetramethylbenzidine (TMB)−H_2O_2 system (Figure 3A). As seen from column 1 and photograph 1, almost no absorbance and color (close to colorless) were observed after incubation with HP_1 and hemin at 450 nm (characteristic absorbance peak of the oxidized TMB), indicating that hemin alone could not open the HP_1 to form the hemin-based DNAzyme. Inspiringly, a strong absorbance and a yellow-colored solution could be obtained when target PNK, HP_1, HP_2, λ-exo$^-$, KF exo$^-$, N.BbvC IA and hemin were present in the incubation solution (column 5 and photograph 5), which mainly derived from the formed peroxidase-mimicking DNAzyme toward the catalytic oxidization of TMB. In contrast, when target PNK (column 2 and photograph 2), HP_1 (column 3 and photograph 3), or N.BbvC IA (column 4 and photograph 4) was absent in the incubation solution, the absorbance was low and the color of the solution was close to colorless. The results in comparison with sample 5 and sample 2 revealed that target PNK could promote the formation of peroxidase-mimicking DNAzyme, whereas the comparative studies with sample 5 and sample 3 could confirm that the absence of HP_1 could not cause the visible color and the strong absorbance (indirectly suggesting the absence of DNAzyme). Meanwhile, the enzyme-assisted isothermal amplification could be also elucidated on the basis of the results of sample 4 and sample 5. Hence, these results indirectly revealed that these two hairpin probes could be employed for the monitoring of PNK activity through DNAzyme-based amplification strategy.

Next, we used electrochemical impedance spectroscopy (EIS) to clarify the secondary concern on the DNAzyme-based catalytic precipitation reaction on AuNP/g-C_3N_3-modified interface because EIS, an effective method to probe the interfacial properties of the modified electrode, is often used for understanding chemical transformations and processes associated with the conductive supports. Typically, the semicircle diameter of EIS equals the electron transfer resistance, R_{et}. which controls the electron transfer kinetics of the redox-probe at the electrode interface. As seen from Figure 3B, the R_{et} at AuNP/g-C_3N_4-modified electrode was small (curve a). After the thiolated HP_1 was assembled on AuNP/g-C_3N_4, the R_{et} increased markedly owing to the repelling effect of the negatively charged DNA toward the negatively charged ferricyanide (curve b). Inspiringly, the change in R_{et} was not almost negligible when the HP_1/AuNP/g-C_3N_4/GCE was incubated with 4-CN-H_2O_2 system (curve c), indicating that the as-prepared electrode could not oxidize the 4-CN even if H_2O_2 was present. However, the resistances slightly increased when the HP_1/AuNP/g-C_3N_4/GCE reacted with the trigger DNA fragment (curve d) and hemin (curve e) in turn. More favorably, a large resistance was achieved after the interaction between the resulting electrode and 4-CN-H_2O_2 system (curve f). The results revealed that the formed DNAzyme could

DOI: 10.1021/acsami.5b01923
ACS Appl. Mater. Interfaces 2015, 7, 8330−8338

catalyze the 4-CN−H_2O_2 system to produce a heavily insulting product and inhibit the electron transfer between the solution and the PEC electrode.

Further, we also utilized the AuNP/g-C_3N_4-modified sensing platform for the monitoring of 50 mU mL^{-1} target PNK (used as an example) in 0.1 M Na_2SO_4 containing 0.1 M Na_2S and 0.05 M Na_2SO_3 based on the photoelectrochemical principle by coupling hairpin-based isothermal amplification with DNAzyme-catalyzed precipitation reaction (Figure 3C). As shown from curve a, a high photocurrent was acquired at AuNP/g-C_3N_4-modified electrode, which could provide convenience for PNK-based inhibition assay. With the introduction of HP_1 (curve b), target-induced trigger DNA fragment (curve c) and hemin (curve d) on the AuNP/g-C_3N_4, the detectable photocurrents gradually decreased, which were in accordance with EIS results. More obviously, the photocurrent largely decreased upon addition of the 4-CN−H_2O_2 system on the DNAzyme-modified interface (curve e). The phenomenon could be explained as follows (i) the precipitated benzo-4-chlorohexadienone was insoluble and greatly hindered the diffusion and electron transfer of Na_2S on the electrode/solution interface to donate electron for the photogenerated holes of g-C_3N_4 and (ii) the precipitation covered on the electrode directly weakened the SPR property of AuNP and the light harvest efficiency of AuNP/g-C_3N_4. On the basis of these results, we might make a conclusion that the AuNP/g-C_3N_4-based PEC sensing platform could be preliminary applied for monitoring of PNK activity by coupling with two hairpin probes and DNAzyme-based biocatalytic precipitation technique.

Optimization of Experimental Conditions. To achieve an optimal analytical performance for our design, some experimental conditions including the concentration of enzymes (e.g., λ-exo$^-$, KF exo$^-$ and N.BbvC IA), the phosphorylation and hydrolysis time for HP_2 by PNK/λ-exo couple, and the reaction time for the isotherm amplification should be investigated. The evaluation was based on the change in the signal-to-noise (S/N) ratio toward the detection system. The detailed results and discussion were described in Figure S3 of the Supporting Information. The optimal experimental parameters were 14-U λ-exo, 30 min for HP_2 phosphorylation and hydrolysis by PNK/λ-exo couple, 1.0-U KF exo$^-$ and 1.8-U N.BbvC IA, and 70 min for the HP_2 mediated signal amplification reaction.

Evaluation of PNK Activity. Under optimal conditions, the ability of quantitative analysis of AuNP/g-C_3N_4-based sensing platform was investigated by assaying different-activity PNK standards with the photoelectrochemical detection method. The PNK activity was monitored with three measurements each in parallel. As shown in Figure 4A, the photocurrents decreased with the increasing PNK activity in the sample, confirming that the designed system could respond to PNK to inhibit the photocurrent signal. A linear dependence between the percentage of photocurrent decrement ($\Delta I/I_0$) and PNK activity was obtained in the range from 2 to 100 mU mL^{-1} (Figure 4B). The linear regression equation was y (μA) = 0.006 × $C_{[PNK]}$ + 0.105 with a correlation coefficient of 0.9948 (n = 21). The detection limit (LOD) was 1.0 mU mL^{-1}, as calculated in terms of the rule of 3× standard deviation over the blank signal. For comparison, we also investigated the analytical properties of using g-C_3N_4-coated electrode without gold nanoparticles for the detection of PNK activity (note: The fabrication of g-C_3N_4-based PNK sensing platform was described in the Supporting Information). As shown in Figure 4C,D, the linear range and LOD were 15−80 and 10.5 mU mL^{-1}. Obviously, the LOD of using the AuNP/g-C_3N_4-coated electrode was lower than those of g-C_3N_4-coated electrode, polyethylene terephthalate (PET) nanochannel-based electronic sensing method,[33] ligase-assisted bioluminescence,[34] gold nanoparticle-enhanced fluorescence polarization assay[35] and molecular beacon-based fluorescence.[36] Such a low LOD was mainly attributed to (i) the exponential amplification features of polymerase/nicking enzyme-assisted isothermal reaction (because the phosphorylation of HP_2 hairpin probe by target PNK and the accompanying solution reaction could induce the generation of numerous trigger DNA fragments to activate the hemin-based DNAzyme in the HP_1 probe)[37−39] and (ii) the photocurrent of AuNP/g-C_3N_4 nanohybrids was high sensitive with local chemical environment and could be drastically inhibited by enzymatic biocatalytic precipitation reaction on the electrode surface.

Inhibition Assay. As is well-known, several reagents including adenosine diphosphate (ADP), ammonium sulfate and sodium hydrogen phosphate can be used as the inhibitors of PNK activity.[40] Typically, the coexistence of ADP with 5′-phosphorylated nucleic acids can trigger a reversible phosphorylation reaction, thus make the phosphate of DNA transfer to ADP molecule. Using ADP as a model inhibitor toward PNK activity, the validity of the as-prepared AuNP/g-C_3N_4 nanohybrids in screening the inhibition of PNK was evaluated through adding the different-concentration ADP into 50 mU mL^{-1} PNK (used as an example) with the above-mentioned system. As shown in Figure 5, the photocurrent responses (ΔI) gradually decreased with the increasing ADP level (Note: the added ADP has no significant effect on the activity of λ-exo[33−36]). Meanwhile, we also observed that addition of 0.6 mM ADP could cause about 50% decrease in ΔI, while the PNK activity was completely inhibited when the concentration of ADP was higher than 2.5 mM, indicating the potential application of the developed assay system for the studies of PNK inhibition.

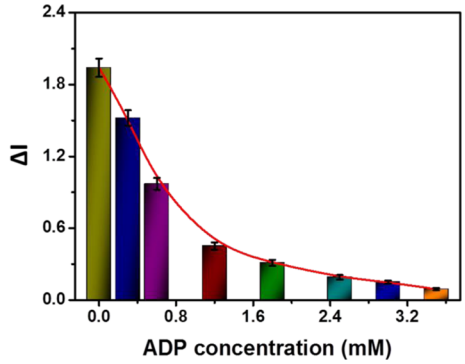

Figure 5. Inhibition effects of ADP on phosphorylation activity of PNK.

4. CONCLUSIONS

In summary, we design a new photoelectrochemical detection platform for ultrasensitive monitoring of PNK activity by using AuNP/g-C_3N_4 nanohybrids as the signal-transduction tags, accompanying with a double-hairpin-based isothermal amplification strategy and an enzymatic biocatalytic precipitation technique. Compared with g-C_3N_4 nanosheets alone, intro-

DOI: 10.1021/acsami.5b01923
ACS Appl. Mater. Interfaces 2015, 7, 8330−8338

duction of gold nanoparticles heavily strengthened the photocurrent responses of g-C_3N_4 nanosheets, and enhanced the detectable sensitivity of the photoelectrochemical sensors based on SPR-enhanced light harvesting and separation of the photogenerated e^-/h^+ pairs. Meanwhile, the AuNP/g-C_3N_4-based PEC detection system did not require the participation of ultraviolet excitation, thus was harmless to biomolecules for the visible-light absorption property and medium band gap (2.7 eV) of g-C_3N_4. More favorably, the HP_2 probe could be phosphorylated by target PNK accompanying with partial digestion by λ-exo to yield an endogenous primer, thereby initiating a solution-phase isothermal amplification reaction to exponentially generate numerous trigger DNA fragments. The released DNA fragments could activated the peroxidase-mimicking DNAzymes on the HP_1 probes to catalyze the precipitation reaction of 4-CN, thus resulting in the decrease of photocurrent responses of the immobilized AuNP/g-C_3N_4 nanohybrids on the electrode. Further, the practicality of system was demonstration through evaluating the inhibition effects of ADP on PNK activity, thus holding great potential application in different routine clinical and biochemical analyses.

■ ASSOCIATED CONTENT

Supporting Information

Fourier-transform infrared spectroscopy of g-C_3N_4 (Figure S1), the predicted secondary structure of hairpin DNA_2 (Figure S2) and the optimization of experimental conditions (Figure S3). This material is available free of charge via the Internet at http://pubs.acs.org.

■ AUTHOR INFORMATION

Corresponding Author

*D. Tang. Phone: +86-591-2286 6125. Fax: +86-591-2286 6135. E-mail: dianping.tang@fzu.edu.cn.

Notes

The authors declare no competing financial interest.

■ ACKNOWLEDGMENTS

Support by the National Natural Science Foundation of China (grant nos. 41176079 & 21475025), the National Science Foundation of Fujian Province (grant no. 2014J07001), and the Program for Changjiang Scholars and Innovative Research Team in University (grant no. IRT1116) is gratefully acknowledged.

■ REFERENCES

(1) Haddour, N.; Chauvin, J.; Gondran, C.; Cosnier, S. Photoelectrochemical Immunosensor for Label-Free Detection and Quantification of Anti-cholera Toxin Antibody. *J. Am. Chem. Soc.* **2006**, *128*, 9693−9698.

(2) Wang, G.; Yu, P.; Xu, J.; Chen, H. A Label-Free Photoelectrochemical Immunosensor Based on Water-Soluble CdS Quantum Dots. *J. Phys. Chem. C* **2009**, *113*, 11142−11148.

(3) Zhao, W.; Ma, Z.; Yu, P.; Dong, X.; Xu, J.; Chen, H. Highly Sensitive Photoelectrochemical Immunoassay with Enhanced Amplification Using Horseradish Peroxidase Induced Biocatalytic Precipitation on a CdS Quantum Dots Multilayer Electrode. *Anal. Chem.* **2012**, *84*, 917−923.

(4) Patolsky, F.; Lichtenstein, A.; Kotler, M.; Willner, I. Photoelectrochemistry with Controlled DNA-Cross-Linked CdS Nanoparticle Arrays. *Angew. Chem., Int. Ed.* **2001**, *40*, 2261−2264.

(5) Wu, Y.; Zhang, Y.; Guo, L. Label-Free and Selective Photoelectrochemical Detection of Chemical DNA Methylation Damage Using DNA Repair Enzymes. *Anal. Chem.* **2013**, *85*, 6908−6914.

(6) Tanne, J.; Schäfer, D.; Khalid, W.; Parak, W.; Lisdat, F. Light-Controlled Bioelectrochemical Sensor Based on CdSe/ZnS Quantum Dots. *Anal. Chem.* **2011**, *83*, 7778−7785.

(7) Qian, Z.; Bai, H.; Wang, G.; Xu, J.; Chen, H. A Photoelectrochemical Sensor Based on CdS-polyamidoamine Nanocomposite Film for Cell Capture and Detection. *Biosens. Bioelectron.* **2010**, *25*, 2045−2050.

(8) Zhao, X.; Zhou, S.; Jiang, L.; Zhou, W.; Chen, Q.; Zhu, J. Graphene-CdS Nanocomposites: Facile One-Step Synthesis and Enhanced Photoelectrochemical Cytosensing. *Chem.—Eur. J.* **2012**, *18*, 4974−4982.

(9) Liang, M.; Wu, S.; Zhu, S.; Guo, L. Photoelectrochemical Sensor for the Rapid Detection of in Situ DNA Damage Induced by Enzyme-Catalyzed Fenton Reaction. *Environ. Sci. Technol.* **2008**, *42*, 635−639.

(10) Yue, Z.; Lisdat, F.; Parak, W.; Hickey, S.; Tu, L.; Sabir, N.; Dorfs, D.; Bigall, N. Quantum-Dot-based Photoelectrochemical Sensors for Chemical and Biological Detection. *ACS Appl. Mater. Interfaces* **2013**, *5*, 2800−2814.

(11) Liang, Y.; Kong, B.; Zhu, A.; Wang, Z.; Tian, Y. A Facile and Efficient Strategy for Photoelectrochemical Detection of Cadmium Ions Based on in Situ Electrodeposition of CdSe Clusters on TiO_2 Nanotubes. *Chem. Commun.* **2012**, *48*, 245−247.

(12) Hu, C.; Zheng, J.; Su, X.; Wang, J.; Wu, W.; Hu, S. Ultrasensitive All-Carbon Photoelectrochemical Bioprobes for Zeptomole Immunosensing of Tumor Markers by an Inexpensive Visible Laser Light. *Anal. Chem.* **2013**, *85*, 10612−10619.

(13) Cui, X.; Wang, Y.; Jiang, G.; Zhao, Z.; Xu, C.; Duan, A.; Liu, J.; Wei, Y.; Bai, W. The Encapsulation of CdS in Carbon Nanotubes for Stable and Efficient Photocatalysis. *J. Mater. Chem. A* **2014**, *2*, 20939−20946.

(14) Wang, X.; Maeda, K.; Thomas, A.; Takanabe, K.; Xin, G.; Carlsson, J.; Domen, K.; Antonietti, M. A Metal-free Polymeric Photocatalyst for Hydrogen Production from Water under Visible Light. *Nat. Mater.* **2009**, *8*, 76−80.

(15) Lee, E.; Jun, Y.; Hong, W.; Thomas, A.; Jin, M. Cubic Mesoporous Graphitic Carbon (IV) Nitride: An All-in-One Chemosensor for Selective Optical Sensing of Metal Ions. *Angew. Chem., Int. Ed.* **2010**, *49*, 9706−9710.

(16) Zhang, X.; Wang, H.; Wang, H.; Zhang, Q.; Xie, J.; Tian, Y.; Wang, J.; Xie, Y. Single-Layered Graphitic-C_3N_4 Quantum Dots for Two-Photon Fluorescence Imaging of Cellular Nucleus. *Adv. Mater.* **2014**, *26*, 4438−4443.

(17) Tang, Y.; Su, Y.; Yang, N.; Zhang, L.; Lv, Y. Carbon Nitride Quantum Dots: A Novel Chemiluminescence System for Selective Detection of Free Chlorine in Water. *Anal. Chem.* **2014**, *86*, 4528−4535.

(18) Zhang, Y.; Schnepp, Z.; Cao, J.; Ouyang, S.; Li, Y.; Ye, J.; Liu, S. Biopolymer-Activated Graphitic Carbon Nitride towards a Sustainable Photocathode Material. *Sci. Rep.* **2013**, *3*, 2163.

(19) Li, R.; Liu, Y.; Cheng, L.; Yang, C.; Zhang, J. Photoelectrochemical Aptasensing of Kanamycin Using Visible Light-Activated Carbon Nitride and Graphene Oxide Nanocomposites. *Anal. Chem.* **2014**, *86*, 9372−9375.

(20) Homola, J. Surface Plasmon Resonance Sensors for Detection of Chemical and Biological Species. *Chem. Rev.* **2008**, *108*, 462−493.

(21) Paracchino, A.; Laporte, V.; Sivula, K.; Grätzel, M.; Thimsen, E. Highly Active Oxide Photocathode for Photoelectrochemical Water Reduction. *Nat. Mater.* **2011**, *10*, 456−461.

(22) Awazu, K.; Fujimaki, M.; Rockstuhl, C.; Tominaga, J.; Murakami, H.; Ohki, Y.; Yoshida, N.; Watanabe, T. A Plasmonic Photocatalyst Consisting of Silver Nanoparticles Embedded in Titanium Dioxide. *J. Am. Chem. Soc.* **2008**, *130*, 1676−1680.

(23) Da, P.; Li, W.; Lin, X.; Wang, Y.; Tang, J.; Zheng, G. Surface Plasmon Resonance Enhanced Real-Time Photoelectrochemical Protein Sensing by Gold Nanoparticle-Decorated TiO_2 Nanowires. *Anal. Chem.* **2014**, *86*, 6633−6639.

DOI: 10.1021/acsami.5b01923
ACS Appl. Mater. Interfaces 2015, 7, 8330−8338

(24) Karimi-Busheri, F.; Rasouli-Nia, A.; Allalunis-Turner, J.; Weinfeld, M. Human Polynucleotide Kinase Participates in Repair of DNA Double-Strand Breaks by Nonhomologous End Joining but not Homologous Recombination. *Cancer Res.* **2007**, *67*, 6619−6625.
(25) Sharma, S.; Doherty, K.; Brosh, R. Mechanisms of RecQ Helicases in Pathways of DNA Metabolism and Maintenance of Genomic Stability. *Biochem. J.* **2006**, *398*, 319−337.
(26) Chen, L.; Zeng, X.; Si, P.; Chen, Y.; Chi, Y.; Kim, D.; Chen, G. Gold Nanoparticle-Graphite-like C_3N_4 Nanosheet Nanohybrids Used for Electrochemiluminescent Immunosensor. *Anal. Chem.* **2014**, *86*, 4188−4195.
(27) Martha, S.; Nashim, A.; Parida, K. Facile Synthesis of Highly Active g-C_3N_4 for Efficient Hydrogen Production under Visible Light. *J. Mater. Chem. A* **2013**, *1*, 7816−7824.
(28) Cheng, N.; Tian, J.; Liu, Q.; Ge, C.; Qusti, A.; Asiri, A.; Al-Youbi, A.; Sun, X. Au-Nanoparticle-Loaded Graphitic Carbon Nitride Nanosheets: Green Photocatalytic Synthesis and Application toward the Degradation of Organic Pollutants. *ACS Appl. Mater. Interfaces* **2013**, *5*, 6815−6819.
(29) Zhu, H.; Chen, X.; Zheng, Z.; Ke, X.; Jaatinen, E.; Zhao, J.; Guo, C.; Xie, T.; Wang, D. Mechanism of Supported Gold Nanoparticles as Photocatalysts under Ultraviolet and Visible Light Irradiation. *Chem. Commun.* **2009**, *48*, 7524−7526.
(30) Bai, X.; Wang, L.; Zong, R.; Zhu, Y. Photocatalytic Activity Enhanced via g-C_3N_4 Nanoplates to Nanorods. *J. Phys. Chem. C* **2013**, *117*, 9952−9961.
(31) Samanta, S.; Martha, S.; Parida, K. Facile Synthesis of Au/g-C_3N_4 Nanocomposites: An Inorganic/Organic Hybrid Plasmonic Photocatalyst with Enhanced Hydrogen Gas Evolution under Visible-Light Irradiation. *ChemCatChem.* **2014**, *6*, 1453−1462.
(32) Little, J. An Exonuclease Induced by Bacteriophage Lambda. II. Nature of the Enzymatic Reaction. *J. Biol. Chem.* **1967**, *242*, 679−686.
(33) Lin, L.; Liu, Y.; Yan, J.; Wang, X.; Li, J. Sensitive Nanochannel Biosensor for T4 Polynucleotide Kinase Activity and Inhibition Detection. *Anal. Chem.* **2013**, *85*, 334−340.
(34) Du, J.; Xu, Q.; Lu, X.; Zhang, C. A Label-Free Bioluminescent Sensor for Real-Time Monitoring Polynucleotide Kinase Activity. *Anal. Chem.* **2014**, *86*, 8481−8488.
(35) Huang, Y.; Chen, J.; Shi, M.; Zhao, S.; Chen, Z.; Liang, H. A Gold Nanoparticle-Enhanced Fluorescence Polarization Biosensor for Amplified Detection of T4 Polynucleotide Kinase Activity and Inhibition. *J. Mater. Chem. B* **2013**, *1*, 2018−2021.
(36) Song, C.; Zhao, M. Real-Time Monitoring of the Activity and Kinetics of T4 Polynucleotide Kinase by a Singly Labeled DNA-Hairpin Smart Probe Coupled with λ Exonuclease Cleavage. *Anal. Chem.* **2009**, *81*, 1383−1388.
(37) Van Ness, J.; Van Ness, L.; Galas, D. Isothermal Reactions for the Amplification of Oligonucleotides. *Proc. Natl. Acad. Sci. U. S. A.* **2003**, *100*, 4504−4509.
(38) Shi, C.; Liu, Q.; Ma, C.; Zhong, W. Exponential Strand-Displacement Amplification for Detection of MicroRNAs. *Anal. Chem.* **2014**, *86*, 336−339.
(39) Lu, L.; Zhang, X.; Kong, R.; Yang, B.; Tan, W. A Ligation-Triggered DNAzyme Cascade for Amplified Fluorescence Detection of Biological Small Molecules with Zero-Background Signal. *J. Am. Chem. Soc.* **2011**, *133*, 11686−11691.
(40) Tang, Z.; Wang, K.; Tan, W.; Ma, C.; Li, J.; Liu, L.; Guo, Q.; Meng, X. Real-Time Investigation of Nucleic Acids Phosphorylation Process Using Molecular Beacons. *Nucleic Acids Res.* **2005**, *33* (e97), 1−6.

DOI: 10.1021/acsami.5b01923
ACS Appl. Mater. Interfaces 2015, 7, 8330−8338